

AFRL-MN-EG-TP-2007-7414

MULTISCALE MODELING OF PARTICLE-SOLIDIFICATION FRONT DYNAMICS, PART III: THEORETICAL ASPECTS AND PARAMETRIC STUDY (PREPRINT)

Justin W. Garvin (AFRL/MNAC)
Computational Mechanics Branch
Air Force Research Laboratory
Eglin AFB, FL 32542

Yi Yang
Falk Corporation
Milwaukee, WI 53208

H. S. Udaykumar
Department of Mechanical
and Industrial Engineering
The University of Iowa
Iowa City, IA 52242



SEPTEMBER 2007

JOURNAL ARTICLE (PREPRINT)

This paper was submitted for publication to the International Journal of Heat and Mass Transfer. One of the authors is a U.S. Government employee working within the scope of his position; therefore, the U.S. Government is joint owner of the work. When published, the publisher may assert copyright. If so, the Government has the right to copy, distribute, and use the work by or on behalf of the U. S. Government. Any other form of use is subject to copyright restrictions.

This work has been submitted for publication in interest of the scientific and technical exchange. Publication of this report does not constitute approval or disapproval of the ideas or findings.

DISTRIBUTION A: Approved for public release; distribution unlimited.
AAC/PA Public Release Approval Confirmation #03-12-07-163;
dated 12 March 2007.

AIR FORCE RESEARCH LABORATORY, MUNITIONS DIRECTORATE

■ Air Force Material Command ■ United States Air Force ■ Eglin Air Force Base

REPORT DOCUMENTATION PAGE					<i>Form Approved OMB No. 0704-0188</i>	
<small>The public reporting burden for this collection of information is estimated to average 1 hour per response, including the time for reviewing instructions, searching existing data sources, gathering and maintaining the data needed, and completing and reviewing the collection of information. Send comments regarding this burden estimate or any other aspect of this collection of information, including suggestions for reducing the burden, to Department of Defense, Washington Headquarters Services, Directorate for Information Operations and Reports (0704-0188), 1215 Jefferson Davis Highway, Suite 1204, Arlington, VA 22202-4302. Respondents should be aware that notwithstanding any other provision of law, no person shall be subject to any penalty for failing to comply with a collection of information if it does not display a currently valid OMB control number.</small>						
PLEASE DO NOT RETURN YOUR FORM TO THE ABOVE ADDRESS.						
1. REPORT DATE (DD-MM-YYYY)		2. REPORT TYPE			3. DATES COVERED (From - To)	
4. TITLE AND SUBTITLE				5a. CONTRACT NUMBER		
				5b. GRANT NUMBER		
				5c. PROGRAM ELEMENT NUMBER		
6. AUTHOR(S)				5d. PROJECT NUMBER		
				5e. TASK NUMBER		
				5f. WORK UNIT NUMBER		
7. PERFORMING ORGANIZATION NAME(S) AND ADDRESS(ES)					8. PERFORMING ORGANIZATION REPORT NUMBER	
9. SPONSORING/MONITORING AGENCY NAME(S) AND ADDRESS(ES)					10. SPONSOR/MONITOR'S ACRONYM(S)	
					11. SPONSOR/MONITOR'S REPORT NUMBER(S)	
12. DISTRIBUTION/AVAILABILITY STATEMENT						
13. SUPPLEMENTARY NOTES						
14. ABSTRACT						
15. SUBJECT TERMS						
16. SECURITY CLASSIFICATION OF:			17. LIMITATION OF ABSTRACT	18. NUMBER OF PAGES	19a. NAME OF RESPONSIBLE PERSON	
a. REPORT	b. ABSTRACT	c. THIS PAGE			19b. TELEPHONE NUMBER (Include area code)	

MULTISCALE MODELING OF PARTICLE-SOLIDIFICATION FRONT DYNAMICS, PART III: THEORETICAL ASPECTS AND PARAMETRIC STUDY

J.W. Garvin¹, Y. Yang², H.S. Udaykumar^{3*}

¹Computational Mechanics Branch, Air Force Research Laboratory, Eglin AFB, Florida 32542

²Falk Corporation, Milwaukee, Wisconsin

³Department of Mechanical and Industrial Engineering
The University of Iowa, Iowa City, IA 52242

ABSTRACT

The development of the solidified microstructure in metal-matrix composites depends on complex interactions between non-planar solidification fronts and multiple particles. The problem is multiscale in nature; the motion of the particle (under the action of a nano-scale disjoining pressure force and a micro-scale viscous drag force) is dynamically coupled with the developing solidification front morphology, which is dependent on a variety of thermal conditions. Using computational techniques discussed in parts I and II, this paper seeks to describe the complicated nonlinear parametric dependencies of the phenomenon. The effects of four of the most important parameters in the particle-solidification front interaction are investigated, i.e. the Hamaker constant, the particle size, the thermal conductivity ratio of the particle to the melt, and the solid-liquid interfacial free energy. By performing simulations using the multiscale approach the dependencies of the critical velocity on these four parameters is clarified.

1. INTRODUCTION

Particle-solidification front interactions are abundant in nature and industrial applications. Examples include: frost heaving in soils [1], cryobiology [2], electrification of clouds [3], and microstructural development in metal-matrix composite manufacture [4-24]. This paper is a culmination of an effort, begun in Parts I and II [17,18] to develop and apply a multiscale model to study the interaction of solidification front with ceramic particles embedded in the melt, a situation that occurs in the formation of microstructures in metal-matrix composites.

* Corresponding author

Email: ush@engineering.uiowa.edu

During the casting process of metal matrix composites, solidification of the metal proceeds in the presence of ceramic particles. A particle that is approached by an advancing solidification front will be engulfed if the solidification velocity exceeds a certain “critical velocity” [7]. For velocities below the critical value the particle is pushed steadily ahead of the front. Determining the conditions under which a particle is pushed or engulfed will aid in the prediction of the overall microstructure of a system and enable control of the solidification process to design desired particle distributions in metal-matrix composite microstructures.

Consider a particle that is being approached by a directionally solidified front (of a pure material) as shown in Figure 1 [17, 18]. As the solidification front approaches the particle distortions in the thermal field can occur when the particle thermal conductivity (k_p) is different from the solidifying melt thermal conductivity (k_l) [10,11]. These distortions will cause the solidifying interface to deviate from planarity and either form a convex protuberance ($k_p/k_l < 1.0$) or a concave trough ($k_p/k_l > 1.0$) underneath the particle [10-12]. A protuberance underneath the particle promotes pushing whereas a trough underneath the particle has a tendency to promote engulfment the particle [12]. In fact, experiments have shown that in cases where a trough has formed ($k_p/k_l > 1.0$) the particle is engulfed nearly all of the time whereas when a protuberance is formed pushing or engulfing can occur [5,6,11] depending on the solidification velocity and other parameters.

As the distance between the solidification front and the particle (d) approaches tens of nanometers a disjoining pressure arises in the gap. The disjoining pressure results due to (repulsive) intermolecular forces that exist in the gap between the two surfaces, namely the solidified material and the ceramic particle. A common continuum representation for the disjoining pressure (Π) is given by [5]:

$$\Pi = \frac{A}{6\pi d^3} \quad (1)$$

where A is the Hamaker constant and d is the distance between the two surfaces. In this work, the disjoining pressure is defined such that a negative Hamaker constant results in a repulsive force between the two interfaces whereas a positive Hamaker constant results in an attractive force between the interfaces. The value (and sign) of the Hamaker constant depends on the system in question, typical values being $\pm 10^{-19}$ Joules.

The Hamaker constant, and hence the disjoining pressure can also be related to the surface free energies of each of the phases involved [5]:

$$A = -4\pi d_0^2 \Delta\gamma \quad (2)$$

where

$$\Delta\gamma = \gamma_{sp} - \gamma_{lp} - \gamma_{sl} \quad (3)$$

where γ_{sp} is the interfacial free energy of the solid(solidification front)-particle interface, γ_{lp} is the liquid-particle interfacial free energy, and γ_{sl} is the solid-liquid interfacial free energy. The d_0 is a constant with the dimensions of length and has a typical value of several molecular diameters [5]. In systems where $\Delta\gamma$ is positive, as the solidification front gets close enough to the particle the existence of a melt layer between the front and particle is energetically favored, in which a repulsive disjoining pressure is formed. The disjoining pressure tends to push the particle away from the front. The opposite is true when the interfacial free energy difference ($\Delta\gamma$) is negative, i.e. the solidification front is attracted to the particle.

The particle reacts to the disjoining pressure and begins to move. Note that if one neglects the volume change upon solidification when starting from an initially quiescent melt there is no fluid flow in the system until the particle begins to move due to the disjoining pressure. The motion of the rejected particle causes a drag that tends to push the particle back towards the solidification front. Overall, the imbalance between the drag and disjoining pressure forces determines whether the particle will be pushed or engulfed. The following four effects impact on the magnitudes of the drag and repulsive disjoining pressure forces:

1. Thermal conductivity ratio: The magnitude of the forces acting on the particle, particularly the drag, depends on the curvature of the solidification front. For example, it has been shown that the drag acting on the particle significantly increases as the k_p/k_l increases [12]. This is due to the large viscous losses in the gap as the solidification front becomes less convex as k_p/k_l increases. This effect is illustrated in pressure contours for various k_p/k_l values shown in Figure 2.

2. Hamaker constant/wettability of the particle: Due to the existence of a disjoining pressure in the melt gap between the particle and the front a change in the melting temperature of the interacting interfaces will result through the Clausius-Clapeyron relation [3]. If $\Delta\gamma > 0$, a layer of

liquid (premelted film) will exist between the solidification front and the particle even when the temperature is lower than that of the bulk melting temperature of the solidifying medium. The solid-liquid interface temperature (T_i) in the presence of such a premelting film is given by [13]:

$$T_i = T_m - \left(\frac{\lambda}{d}\right)^3 T_m \quad (4)$$

where λ is an interaction length scale and T_m is the bulk melting temperature.

The existence of a premelted film and the interfacial temperature depression can have a significant effect on front-particle interaction. The premelting effect alters the shape of the solidification front and hence changes the way the forces behave. If one assumes premelting, the solidification front deforms to accommodate a liquid layer – hence affecting the forces that act on the particle (see Figure 3) [14]. As shown in Figure 3, the solidifying interface begins to bend around the particle in order to accommodate the liquid layer. This change in curvature of the front leads to significant changes in the forces that act on the particle.

3. Solid-liquid interfacial tension effect through the Gibbs-Thomson condition: The solid/liquid interfacial free energy of the solidification front also affects the shape and curvature of the solidifying interface. The solid/liquid interfacial free energy enters the problem through the modification of the melting temperature in Eq. (4) as follows [15,16]:

$$T_i = T_m - \left(\frac{\lambda}{d}\right)^3 T_m - \frac{\gamma_{sl}\kappa}{\rho H_{sl}} T_m \quad (5)$$

The last term on the right accounts for the Gibbs-Thomson effect. The γ_{sl} is the solid-liquid interfacial free energy of the solidification front, κ is the curvature of the solidification front, ρ is the density of the melt, and H_{sl} is the latent heat of fusion per unit mass. The Gibbs-Thomson effect reduces the magnitude of the curvature of the solidification front (i.e. it tends to flatten the front out). Hence, the forces will be affected and the critical velocity will change.

4. Particle size (R_p): The particle radius also plays a role in the determination of the critical velocity. As the particle radius increases the drag on the particle increases at a faster rate than the repulsive disjoining pressure force acting on the particle. This is simply due to the fact that the repulsive force only acts over a small portion of the particle surface (i.e. the portion where the gap is small enough so that the disjoining pressure effects become important), whereas the fluid drag acts on the entire particle surface. Models and experiments have both shown that the critical velocity is inversely proportionally to the particle radius [4-6].

All of the work on particle-front interactions up to now has relied on focusing on one parameter or another, mostly in a steady-state pushing mode [6,7,10,13,15,16]. There have been a few dynamic models [4, 8, 22] of particle-solidification front interactions but they too have relied heavily on various assumptions to make the problem tractable (e.g. no premelting, no surface tension effects, simplified solidification models and simplified force models). This study includes all of the main parameters involved (the particle radius (R_p), the k_p/k_l , the Hamaker constant, and the solid-liquid interfacial energy) and illustrates how these effects, when acting in concert, makes for a highly sensitive dynamical problem. The methodology for modeling and solving the resulting multiscale problem was detailed in Part I [17]. In Part II [18] the mechanism for determination of the critical velocity was elucidated. Here, a detailed parameteric study is performed to clarify the dependence of the critical velocity on each of the above-listed four main parameters that influence the particle-front interactions. In addition, the physics behind the dependency of the critical velocity on the parameters listed above is also clarified.

2. COMPUTATIONAL SETUP

The computational setup is shown in Figure 4. The solidification front moves upward and approaches the particle. In order to capture all of the essential physics of the problem in a multiscale setting, the computational domain needs to be divided into two different regions. In the “outer” region (comprising of the particle and the flow and thermal field surrounding it) the full 2D flow and heat transport equations are solved. In the “inner” region (comprising of the gap between the particle and the front) a lubrication equation is solved by making a thin gap assumption ($d \ll R_p$). The solutions of the “inner” and “outer” regions are then coupled through a “matching” region by supplying boundary conditions to each region. The fully coupled solution in the two regions proceeds in tandem over each time step. The forces on the particle are evaluated using the composite solution (i.e. inner and outer region solutions) and the particle is moved in Lagrangian fashion. The calculation of the dynamics of the particle-front interaction

takes into account all of the most important physical mechanisms in a multiscale setting. The details of the numerics are discussed in parts I and II [17,18] and will not be discussed in this paper.

3. RESULTS AND DISCUSSION

3.1. Physical Description of the Pushing-Engulfing Transition Based on Front Curvature Arguments

The curvature of the solidification front directly beneath the particle (henceforth referred to as the “tip” of the solidification front) has a significant impact on the critical velocity. Figure 5 shows the evolution of the particle-front system for a two different cases, one where the particle is approached by an initially planar front (Figure 5(a), (c)) and is pushed ahead of it and the other where the particle becomes engulfed by the front (Figure 5(b),(d)).

Case 1 (Pushing): Figures 5 (a) and (c) respectively show the particle velocity (v_p) versus time (t) and the ratio of the tip curvature to R_p^{-1} (also referred to as the dimensionless tip curvature κ_t^*) versus time for a case where the particle is pushed by the front, i.e. $R_p = 1$ micron, $A = -8 \times 10^{-19}$ Joules, $\lambda = 3.5 \times 10^{-10}$ meters, $\gamma_{sl} = 0$, and a solidification velocity (v_s) of 200 μ/s . As shown in Figure 5 (c), for this case the tip curvature starts out at a value approximately half the particle radius and then settles to a steady mean value not long after the start of the particle-front interaction. Correspondingly, as can be seen from Figure 5 (a), the particle velocity significantly increases and begins to oscillate at a value commensurate with the solidification front velocity, i.e. it enters a pushing mode.

Case 2 (Engulfment): Figures 5 (b) and (d) denote the particle velocity versus time and the tip curvature versus time for the same system but for a somewhat higher solidification velocity at which the particle is engulfed by the front, i.e. $v_s = 215 \mu/s$. In contrast with Case 1, in Figure 5 (d), the curvature of the tip of the solidification front also starts out around 2.0 but then reaches a maximum and begins to decrease. The tip curvature continues to decrease until it reaches a value of around -1. This indicates that the shape of solidification front is conforming to the shape of the particle.

The decrease in the tip curvature in Figure 5(d) is due to the premelting effect. Since there is a tendency, according to the premelting theory, for a liquid layer to persist in the gap between the particle and the front, the tip of the solidification front begins to flatten and assume a concave shape in conformity with the shape of the particle. The flattened solidification front tip results in a larger drag since there will be larger viscous losses in the melt flowing into the narrow gap. The large drag causes the particle to slow down, as can be seen in Figure 5 (b). With further flattening, the curvature of the tip becomes such that the drag outweighs the disjoining pressure forces. Once the drag becomes the dominant force, the particle begins to slow down to an eventual stop leading to engulfment. On the other hand, in the case where the particle is pushed ahead of the front, the particle achieves a high enough velocity, relative to the tip velocity, so that the gap thickness never reaches a point where premelting effects dominate. Then the interface tip curvature does not decrease significantly (as seen in Figure 5(c)) and hence the drag force does not dominate the repulsive disjoining force

A further aspect of the effect of solidification front curvature needs to be considered, i.e. the curvature of the front prior to contact with the particle. Figure 6 plots the tip curvature versus time for both the pushing and engulfment cases that were described above. It is seen that the tip curvature in the pushing (i.e. $v_s = 200 \mu/s$, Figures 5(a), (c)) case starts out as a higher value than in the engulfment case ($v_s = 215 \mu/s$, Figures 5(b), (d)). In other words, the pushing case has a more pronounced protuberance underneath the particle than the engulfment case even before the

particle begins to interact with the front. For the higher Stefan number, $Ste = \frac{k_l G_l}{\rho H_{sl} v_s}$ (where

G_l is the thermal gradient in the liquid), corresponding to the lower solidification velocity the front senses the insulating particle earlier and deviates from planarity before approaching the particle. For the higher front velocity, since the Stefan number is low, the front remains nearly planar as it approaches the particle.

In determining whether the particle is pushed or engulfed by the front, there is a delicate balance between the development of a premelted layer, the speed of the solidification front, and other parameters (particle size, thermal conductivity, solid-liquid interfacial energy) that affect how the solidification front evolves in time. Each of these effects impact on the curvature of the front directly beneath the particle, which as discussed above correlate with whether the particle is pushed or engulfed by the front. Therefore, a parametric study is performed using the numerical methodology developed in Parts I and II to study how the critical velocity depends on the most

significant solidification process and material parameters. In order to obtain the critical velocity for each parameter value several runs were made to identify points in the parameter space where the system shows a transition from pushing to engulfment and the boundary between the two behaviors is demarcated. To condense data, only those points that fall on the boundary between pushing and transition are shown in the figures. In general, the number of cases to be run was decreased considerably by judicious choice of parameter values and by observing the trends seen for each parameter value. The final results only are presented in the following parametric study in order to make a concise presentation of the data and insights.

3.2. Critical velocity as a function of particle size (R_p)

First, the dependence of the critical velocity on the particle radius (R_p) is studied. Figure 7 shows the solidification velocity far from the front (v_s), which in directional solidification terminology is v_{pull} , (the velocity with which the sample is “pulled”), versus R_p . Other parameters are $k_p/k_l = 0.01$, $A = -8 \times 10^{-19}$ Joules, $\lambda = 3.5 \times 10^{-10}$ meters, and $\gamma_{sl} = 0$. Several cases were run for each R_p and the points plotted demarcate the transition from pushing to engulfment. The solid line represents a curve-fit to the transition between pushing and engulfment behavior that describes the variation of the critical velocity with the particle radius. From Figure 7 it is observed that there is an inverse relationship between the critical velocity and the particle radius with the curve-fit providing the expression: $V_{CR} = 207 / R_p$ (where V_{CR} is in μ/s and R_p is in microns). This computed dependency agrees with the experimentally observed relationship $V_{cr} \propto R_p^{-1}$ [4,5].

3.3. Critical velocity as a function of particle thermal conductivity (k_p/k_l)

The general effect of k_p/k_l on the critical velocity is well established in the particle-solidification front interaction literature. It is well known and it can be physically explained that when $k_p/k_l < 1$ particle pushing can result, while for $k_p/k_l > 1$ engulfment is the most likely result. However, it is difficult to precisely quantify the specific effect of the k_p/k_l experimentally since changing the k_p/k_l would require changing the materials under study and consequently the Hamaker constant, λ . From theoretical work, Shangguan *et al.* [6] and Catalina *et al.* [4] suggest that the critical velocity is inversely proportional to the k_p/k_l . More specifically, they obtain a critical velocity of [6]:

$$V_{CR} = \frac{7a_o\Delta\gamma}{64 * 3\mu R_p \left(\frac{k_p}{k_l} \right)} \quad (6)$$

where a_o is the molecular diameter and is on the order of Angstroms in size and μ is the dynamic viscosity of the melt.

Note that in determining the critical velocity obtained in Eq. (6) simplifying assumptions were made to render the analysis tractable. In that work the premelting effect was not included in Eq. (6) which required an *ad hoc* cut-off gap thickness to be invoked in order to distinguish between pushing and engulfment (see references [4,6] for discussion of a gap thickness cut-off). The present modeling and solution approach allow for the removal of limitations inherent in the analysis presented in [6]. Therefore, the above expression for the dependency of critical velocity on thermal conductivity ratio is re-examined with the current multiscale approach.

Figure 8 compares the variation of the critical velocity with respect to the k_p/k_l (with $A = -8 \times 10^{-19}$ Joules, $\lambda = 3.5 \times 10^{-10}$ meters, $R_p = 1$ micron, and $\gamma_{sl}=0$) using the current method to that of the previously suggested inverse relationship due to Shangguan *et al.* [6]. From Figure 8, in agreement with Shangguan *et al.* [6], the critical velocity decreases as the k_p/k_l increases. This dependency can be explained from the physics of the problem, in that larger k_p/k_l causes the solidification front to flatten out with the front eventually becoming concave underneath the particle when k_p/k_l becomes greater than one (see Figure 2). The drag therefore increases as k_p/k_l increases, which tends to promote engulfment. Since engulfment is more likely to occur when k_p/k_l increases the critical velocity decreases with increasing k_p/k_l . However, Figure 8 shows that the functional form of the relationship between the critical velocity and the k_p/k_l is quite different from that given by Shangguan *et al.* [6] in Eq. (6). Note that the functional relationship indicated by the present calculations takes into account the delicate interplay between the drag force and the disjoining pressure force. The strength of these forces is highly dependent on the shape of the solidification front. The k_p/k_l greatly influences the shape of the solid-liquid interface. However, the k_p/k_l value is not the only factor that influences the shape (in particular the curvature) of the solidification front. Premelting and Gibbs-Thomson effects also play a role. In the work of Shangguan *et al.* [6], premelting effects were not included and hence the solid-liquid interface shape was influenced solely by k_p/k_l effects.

3.4. Critical velocity as a function of particle wettability (Hamaker constant (A))

As mentioned before, the Hamaker constant is related to the interfacial free energy difference between the three phases (solid, liquid, and particle) through Eq. (2). As pointed out for k_p/k_l in Section 3.3, experimentally isolating the effect of the Hamaker constant on the critical velocity also proves to be difficult. However, a comparison can still be made with theoretical models, particularly those of Shangguan *et al.* [6].

Figure 9 plots the solidification velocity far from the front (v_s) versus the Hamaker constant (A) for systems where $R_p = 1$ micron, $\gamma_{sl} = 0$, and $k_p/k_l = 0.01$. It is seen that as A becomes more negative the critical velocity increases. This is to be expected, since as the value of the disjoining pressure in Eq. (1) becomes more negative, the repulsive force between the particle and the solidification front becomes greater which tends to promote pushing. From Eq. (1), it would appear likely that the Hamaker constant affects the critical velocity in a linear fashion, since the disjoining pressure is linearly related to the Hamaker constant. This is also suggested by the model presented by Shangguan *et al.* [6]. In fact the present calculations deviate only slightly from linearity. The reason for the slight deviation is due to the fact that changing the Hamaker constant also changes the premelting parameter, λ , through the equation [13]:

$$\lambda = \sqrt[3]{\frac{A}{6\pi\rho H_{sl}}} \quad (7)$$

where, ρ is the density of the melt and H_{sl} is the latent heat of fusion of the melt per unit mass.

The disjoining pressure in the premelted layer and the interface temperature are related via the Clausius-Claperyon equation. The change in the solidification front morphology due to the depression of interface temperature causes the forces acting on the particle to be altered and this effect is reflected in the deviation from linearity of the curve in Figure 9. In the work of Shangguan *et al.* [6], no premelting was assumed and therefore a linear dependence was found.

3.5. Critical velocity as a function of solid-liquid surface tension (γ_{sl})

In the cases computed so far the interfacial temperature on the melting temperature was not included. In reality, the curvature of the solidification front affects the temperature at which the solidification front solidifies through the Gibbs-Thomson effect, viz.:

$$T_i = T_m - \frac{\gamma_{sl}\kappa}{\rho H_{sl}} T_m - \left(\frac{\lambda}{d}\right)^3 T_m \quad (8)$$

where T_m is the bulk melting temperature and κ is the solidification front curvature.

Non-dimensionalizing T_m by $G_L R_p$, d by d_c , and κ by $1/R_p$ gives:

$$T_i^* = -\Gamma \kappa^* - \left(\frac{\lambda}{d_c d^*}\right)^3 \frac{T_m}{G_L R_p} \quad (9)$$

Where $\Gamma = \frac{\gamma_{sl} T_m}{G_L R_p^2 \rho H_{sl}}$ is a non-dimensional capillarity parameter for the solid-liquid interface.

Interfacial tension at the solid-liquid interface hinders the formation of a bump underneath the particle. Figure 10 illustrates how the critical velocity varies as a function of Γ . In these cases $k_p/k_l = 0.01$, $A = -8 \times 10^{-19}$ Joules, $\lambda = 3.5 \times 10^{-10}$ meters, and $R_p = 1.0 \times 10^{-6}$ meters. From Figure 10, it is seen that as Γ increases, the critical velocity decreases. The reason for this is that the convexity of the interface underneath the solidification front is less pronounced as Γ increases, i.e. higher curvatures are discouraged by capillary effects. Since the solidification front is flatter in the case of higher Γ , the pressure losses in the gap are higher and hence the drag is higher. Since the drag force tends to promote engulfment, for higher Γ the particle will more likely be engulfed, and hence the critical velocity is smaller. Figure 10 also indicates that the critical velocity is nearly a linear function of Γ .

4. CONCLUSIONS

The curvature of the tip of solidification front, and its evolution in time, has a direct effect on whether the particle is pushed or engulfed. A high positive (convex) curvature tends to promote pushing since the fluid drag decreases as the curvature increases. The curvature of the interface, however, is a complex time-dependent function of the thermal-fluid transport combined with interfacial phenomena such as premelting layers and the resulting pressure and temperature in the layers, the surface energies of the interacting interfaces etc. This computational study has clarified, by means of a detailed parametric analysis the following effects of the most important parameters in particle-front interactions:

- 1) Effects of pull speed in the directional solidification process: As v_s increases the difference between the diffusion rate and the solidification rate decreases (i.e. the Stefan number decreases) and hence the distance at which the particle is felt by the front is decreased. This causes the solidification front to remain flat until the presence of the particle begins to distort the temperature field. This is, arguably, a small effect unless v_s is very high. The higher the v_s , the smaller the curvature of the front as it approaches the particle. This fact, along with the fact that the particle velocity may not have time to catch up with and outstrip the high solidification velocity makes the particle more prone to engulfment.
- 2) Effects of the particle velocity (v_p) relative to the tip velocity (v_t): If the tip velocity is high enough that the particle is not pushed away sufficiently from the front, the effects of premelting in the thin melt gap take over; then the curvature of the tip will decrease and the particle will begin to experience a large drag. This drag further impedes the motion of the particle until eventual engulfment ensues.
- 3) Effects of particle thermal conductivity (k_p/k_l): When k_p/k_l is different from unity the particle distorts the thermal field of the system which causes a deformation of the solidification front. The smaller the k_p/k_l , the larger the critical velocity.
- 4) Effect of the Hamaker constant: The Hamaker constant, A , affects the solidification tip curvature through its effect on the premelted layer. If a layer of liquid is energetically favored to exist between the particle and the solidification front, the curvature of the tip will change to accommodate such a layer. The critical velocity increases as A becomes more negative due to the larger repulsive force that acts on the particle.

- 5) Solid-liquid interfacial energy Effects (Γ): The interfacial free energy of the solid-liquid interface, γ_{sl} (or Γ in non-dimensional terms), controls the curvature of the solidification front. Increasing Γ tends to enhance the smoothness of the solidification front. Since the interface flattens, the critical velocity decreases as Γ increases.

The above effects working in a coupled and dynamic fashion make the problem of particle-solidification front interactions a very challenging one to analyze from a theoretical standpoint. The computational methodology developed in Part I [17] has enabled the detailed parametric study presented in this paper. The results obtained provide insights and quantification of the dependencies of the critical velocity on the most important thermo-physical properties in the particle-front interaction system.

5. ACKNOWLEDGEMENTS

This work was supported by a National Science Foundation CAREER Award (CTS-0092750) to the third author.

6. CONCLUSION

1. A.W. Rempel, J.S. Wettlaufer, M.G. Worster, "Premelting dynamics in a continuum model of frost heave", *Journal of Fluid Mechanics*, v498, n10, Jan. 2004, pp. 227-244.
2. L. Mao, H.S. Udaykumar, J.O.M. Karlsson, "Simulation of micro-scale interaction between ice and biological cells", *International Journal of Heat and Mass Transfer*, v46, n26, Dec. 2003, p. 5123-5136.
3. J.G. Dash, Fu Haiying, J.S. Wettlaufer, "The premelting of ice and its environmental consequences", *Reports on Progress in Physics*, v58, n1, Jan. 1995, p. 115-167.
4. A.V. Catalina, S. Mukherjee, D.M. Stefanescu, "Dynamic model for the interaction between a solid particle and an advancing solid/liquid interface", *Metallurgical and Materials Transactions A*, v31, n10, Oct. 2000, pp. 2559-2568.
5. R. Asthana, S.N. Tewari, "Second phase particle-solidification front interactions: an evaluation of theoretical models", *Processing of Advanced Materials*, v3, n3, Sept. 1993, pp. 163-180.

6. D. Shangguan, S. Ahuja, D.M. Stefanescu, "An analytical model for the interaction between an insoluble particle and an advancing solid/liquid interface", *Metallurgical Transactions A (Physical Metallurgy and Materials Science)*, v23A, n2, Feb. 1992, pp. 669-680.
7. D.R. Uhlmann, B. Chalmers, K.A. Jackson, *Journal of Applied Physics*, v. 35, 1964, p. 286.
8. J.W. Garvin and H.S. Udaykumar, "Particle-solidification front dynamics using a fully coupled approach, part I: methodology", *Journal of Crystal Growth*, v. 252, n1-3, May 2003, pp. 451-466.
9. J.W. Garvin and H.S. Udaykumar, "Particle-solidification front dynamics using a fully coupled approach, part II: comparison of drag expressions", *Journal of Crystal Growth*, v252, n1-3, May 2003, pp. 467-479.
10. A.A. Chernov, D.E. Temkin, A.M. Mel'nikova, *Sov. Phys. Crystallogr.*, 22(6), 1977, pp. 656.
11. A.M. Zubko, V.G. Lobanov, V.V. Nikonova, *Sov. Phys. Crystallogr.*, 18(2), 1973, pp. 239.
12. J.W. Garvin and H.S. Udaykumar, "Drag on a particle being pushed by a solidification front and its dependence on thermal conductivities", *Journal of Crystal Growth*, v267, n3-4, July 2004, pp. 724-737.
13. A.W. Rempel and M.G. Worster, "The interaction between a particle and an advancing solidification front", *Journal of Crystal Growth*, v 205, n3, 1999, pp. 427-440.
14. J.W. Garvin and H.S. Udaykumar, "Effect of a premelted film on the dynamics of particle-solidification front interactions", *Journal of Crystal Growth*, v290, n2, May 2006, pp. 602-614.
15. A.W. Rempel and M.G. Worster, "Particle trapping at an advancing solidification front with interfacial-curvature effects", *Journal of Crystal Growth*, v223, n3, March 2001, pp. 420-432.

16. L. Hadji, "Axisymmetric shapes and forces resulting from the interaction of a particle with a solidifying interface", *Physical Review E*, v66, n4, Oct. 2002, pp. 041404.
17. J.W. Garvin, Y. Yang, H.S. Udaykumar, "Multiscale modeling of particle-solidification front dynamics, part I: Methodology", *International Journal of Heat and Mass Transfer* (accepted).
18. J.W. Garvin, Y. Yang, H.S. Udaykumar, "Multiscale modeling of particle-solidification front dynamics, part II: Pushing-engulfment transition", *International Journal of Heat and Mass Transfer* (accepted).
19. J. Potschke and V. Rogge, "On the behaviour of foreign particles at an advancing solid-liquid interface", *Journal of Crystal Growth*, v94, n3, March 1989, pp. 726-738.
20. S.N. Omenyi and A.W. Neumann, *Journal of Applied Physics*, v47(9), 1976, pp. 3956.
21. G. Kaptay, "Interfacial criterion of spontaneous and forced engulfment of reinforcing particles by an advancing solid/liquid interface", *Metallurgical and Materials Transactions A*, v32A, April 2001, pp. 993.
22. A. Borsik, K.K. Kelemen, G. Kaptay, "A dynamic model of ceramic particle-solidification front interaction", *Materials Science Forum*, v. 414-415, pp. 371-76 (2003).
23. Y. Yang, J.W. Garvin, H.S. Udaykumar, "Sharp interface simulation of interaction of a growing dendrite with a stationary solid particle", *International Journal of Heat and Mass Transfer*, v48, n25-26, p. 5270-83 (2005).
24. L. Mao, H.S. Udaykumar, J.O.M. Karlsson, "Simulation of micro-scale interaction between ice and biological cells", *International Journal of Heat and Mass Transfer*, v.46, n26, pp.5123-36, (2003).

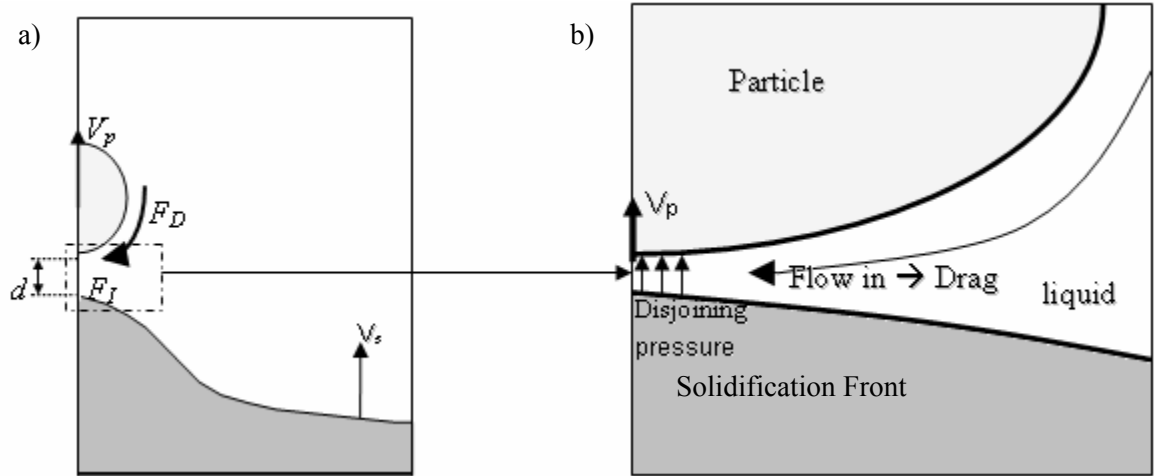


Figure 1. (a) Schematic of the overall system. (b) Schematic of the zoomed-in box in (a) illustrating the different mechanisms involved in the particle-solidification front interaction. As the solidification front approaches the particle, the disjoining pressure starts to push the particle (if $\Delta\gamma > 0$). Fluid then flows in to replenish the gap which results in a drag force.

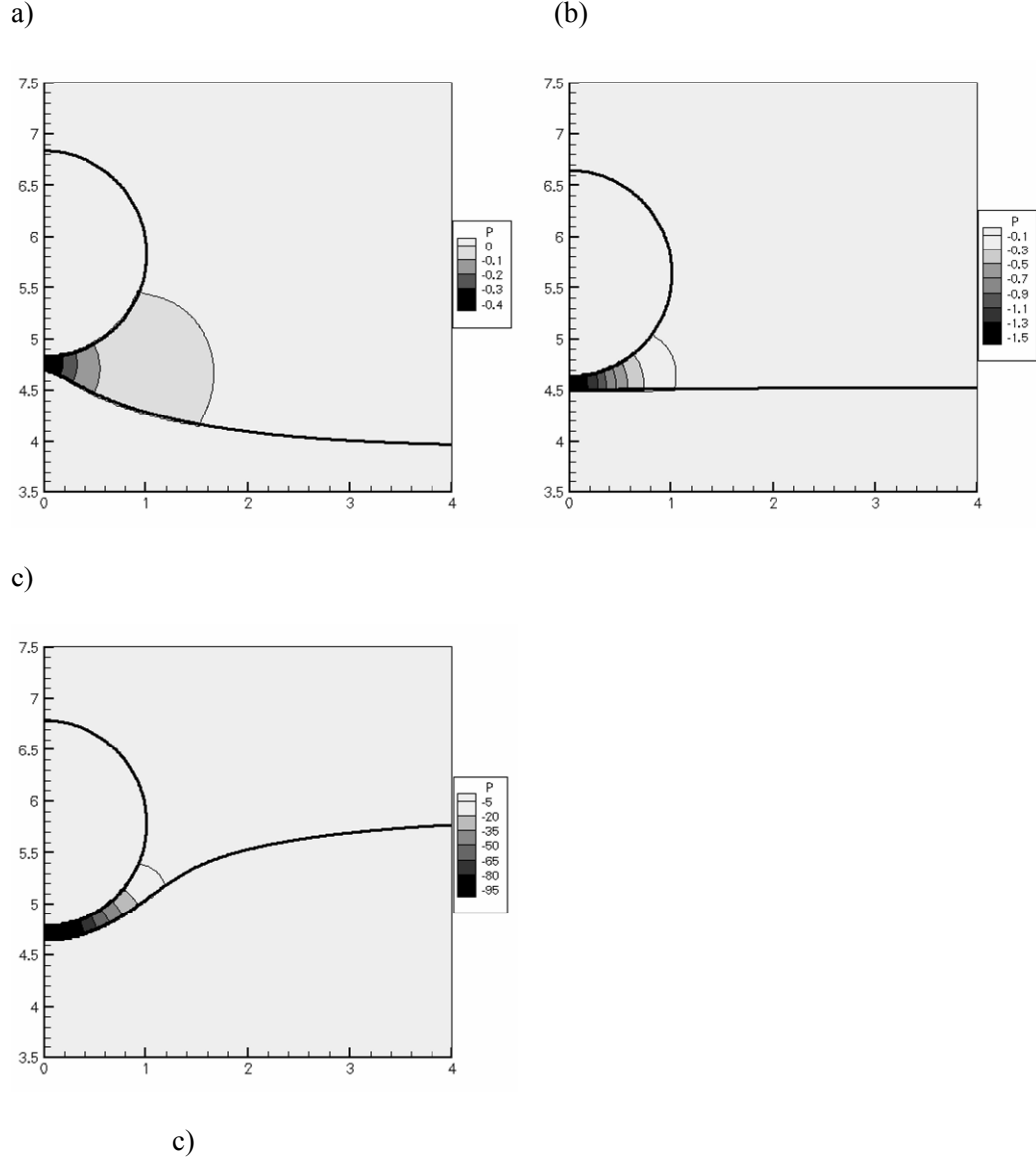


Figure 2: Interface shape and pressure contours for cases where the solidification front approaches a particle with the properties: a) $k_p/k_l = 0.01$, b) $k_p/k_l = 1.0$, and c) $k_p/k_l = 30.0$. The indicated pressure is non-dimensional.

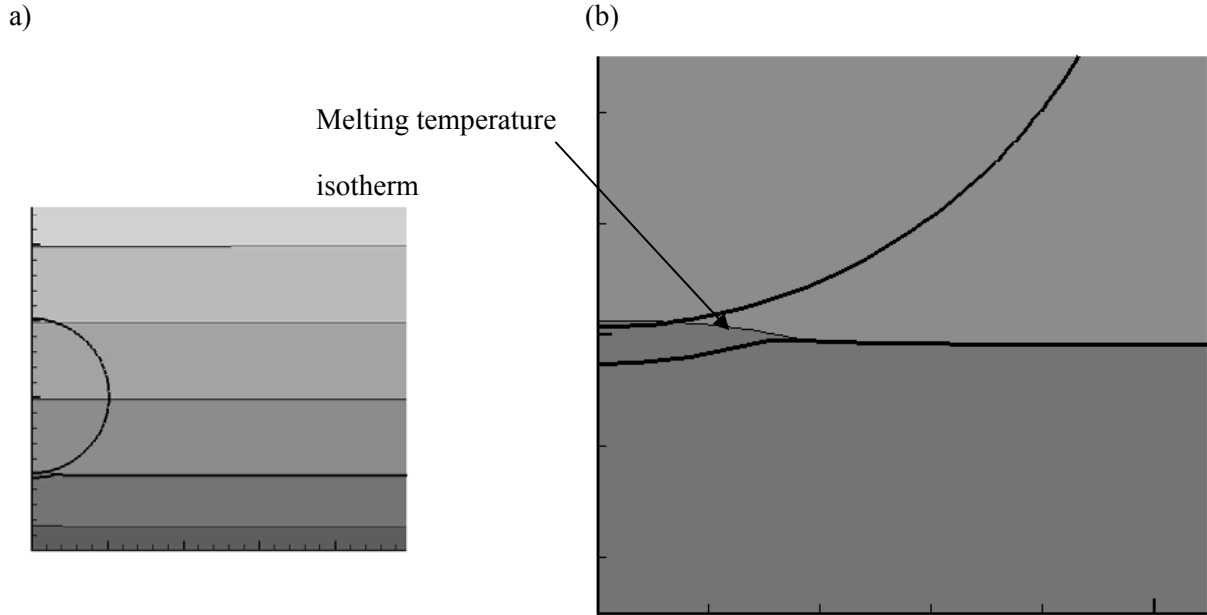


Figure 3: Premelting effect on the solidification front (interfaces are shown by bold curves and the contours are of temperature are also shown in the figures): (a) Overall view and (b) Zoomed-in view of the interface. The premelting effect leads to a loss of planarity of the interface.

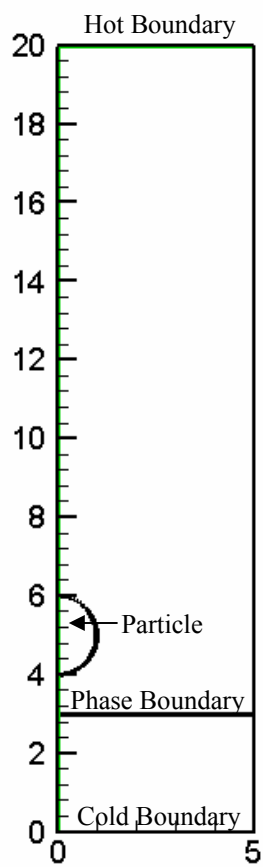


Figure 4. Initial system setup for the computations performed.

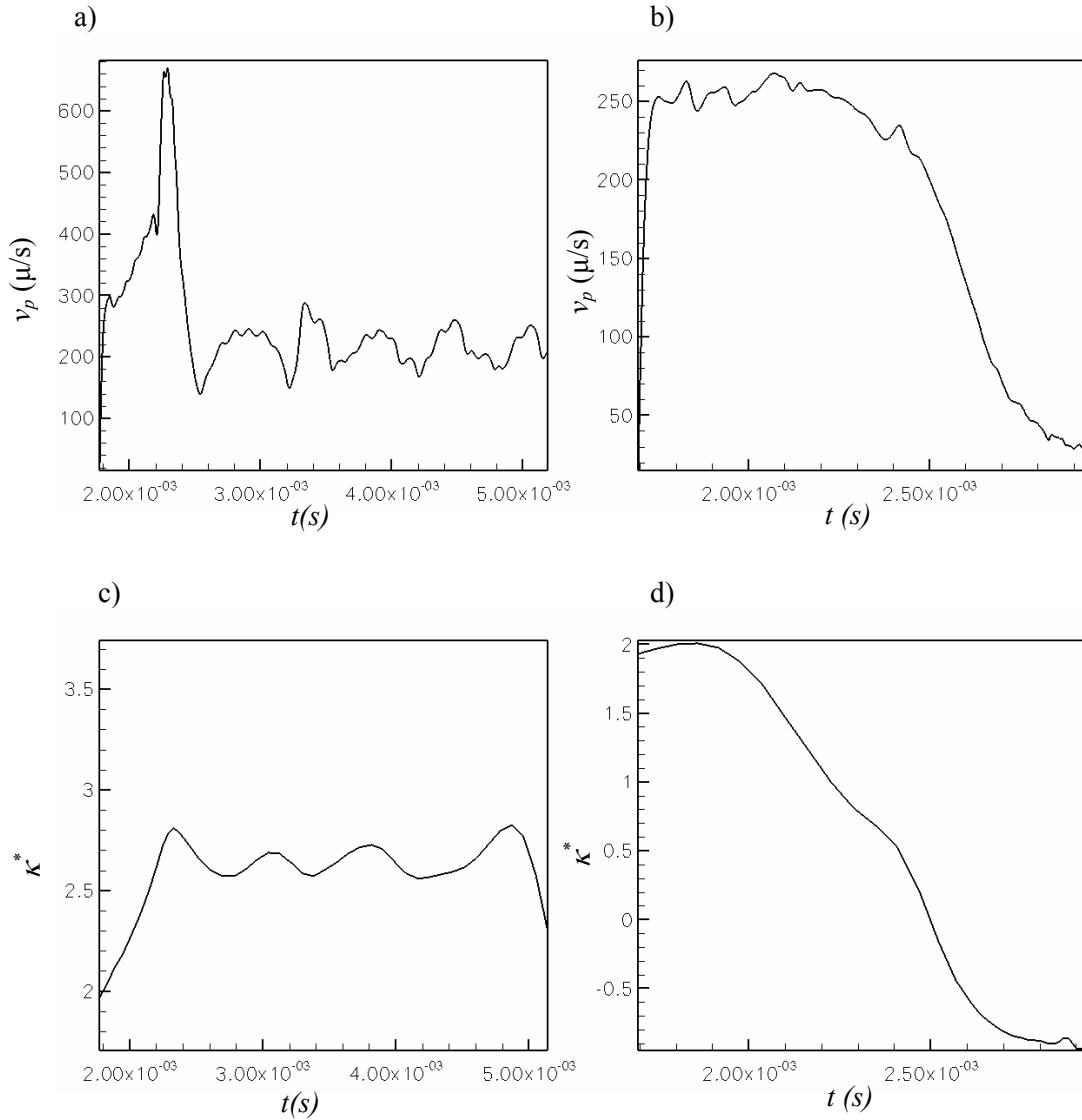


Figure 5: Relationship between interface curvature, velocity and the pushing/engulfment of a particle when approached by a solidification front. (a) Case 1 - Particle velocity versus time for the pushing case $k_p/k_l = 0.01$, $R_p = 1.0 \times 10^{-6}$ m, $A = -8 \times 10^{-19}$ Joules, $\lambda = 3.5 \times 10^{-10}$ meters, $v_s = 200$ microns/second. (b) Case 2- particle velocity versus time for the case where the particle is engulfed by the front; $k_p/k_l = 0.01$, $R_p = 1.0 \times 10^{-6}$ m, $A = -8 \times 10^{-19}$ Joules, $\lambda = 3.5 \times 10^{-10}$ meters, $v_s = 215$ microns/second. (c) and (d) Non-dimensional curvature versus time corresponding to (a) and (b) respectively.

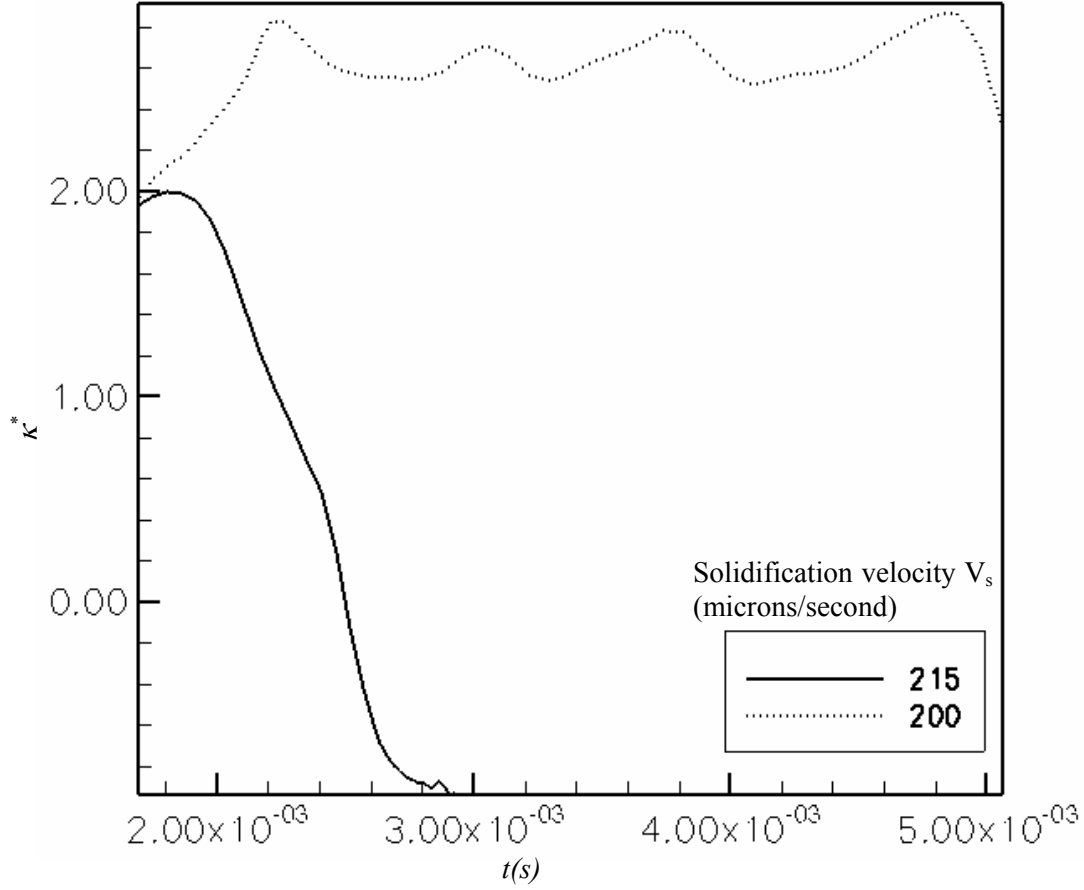


Figure 6: Non-dimensional curvature versus time. For the solid line (engulfed case): $k_p/k_l = 0.01$, $R_p = 1.0 \times 10^{-6}$ m, $A = -8 \times 10^{-19}$ Joules, $\lambda = 3.5 \times 10^{-10}$ meters, $V_s = 215$ microns/second. For the dotted line (pushed case): $k_p/k_l = 0.01$, $R_p = 1.0 \times 10^{-6}$ m, $A = -8 \times 10^{-19}$ Joules, $\lambda = 3.5 \times 10^{-10}$ meters, $v_s = 200$ microns/second.

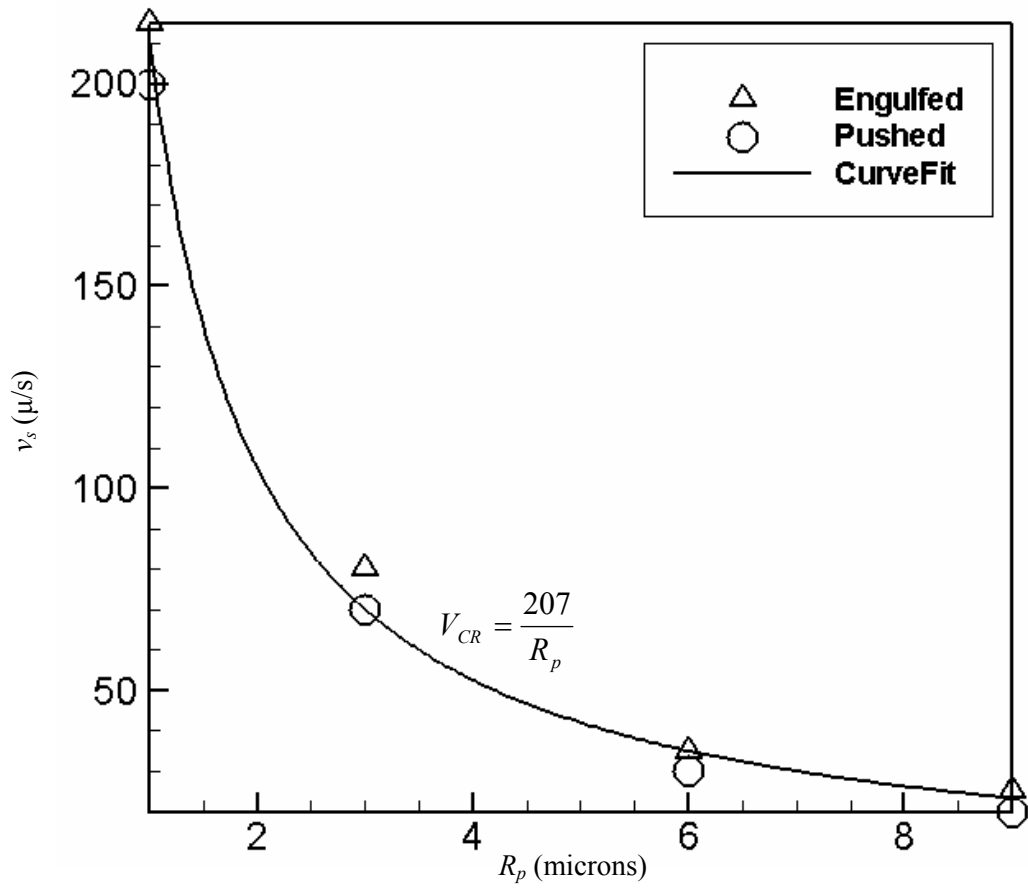


Figure 7: Identification of the critical velocity dependency on the particle radius (v_s vs. R_p) The other parameters are held fixed at $k_p/k_l = 0.01$, $A = -8.0 \times 10^{-19}$ J, $\lambda = 3.5 \times 10^{-10}$ m, and $\gamma_{sl} = 0.0$.

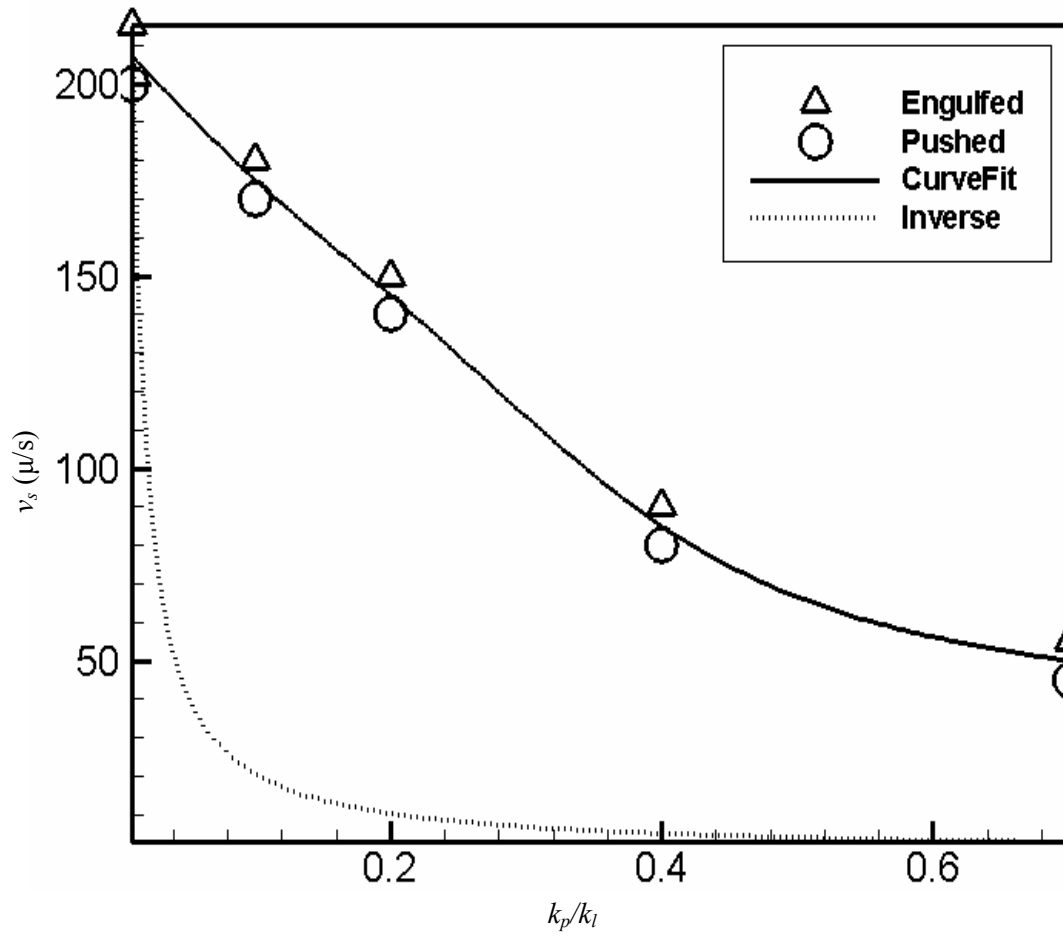


Figure 8: Dependence of the critical velocity on the ratio of thermal conductivity of the particle to the melt, v_s vs. k_p/k_l . The other parameters are held fixed at $R_p = 1$ micron, $A = -8.0 \times 10^{-19}$ J, $\lambda = 3.5 \times 10^{-10}$ m, and $\gamma_{sl} = 0.0$.

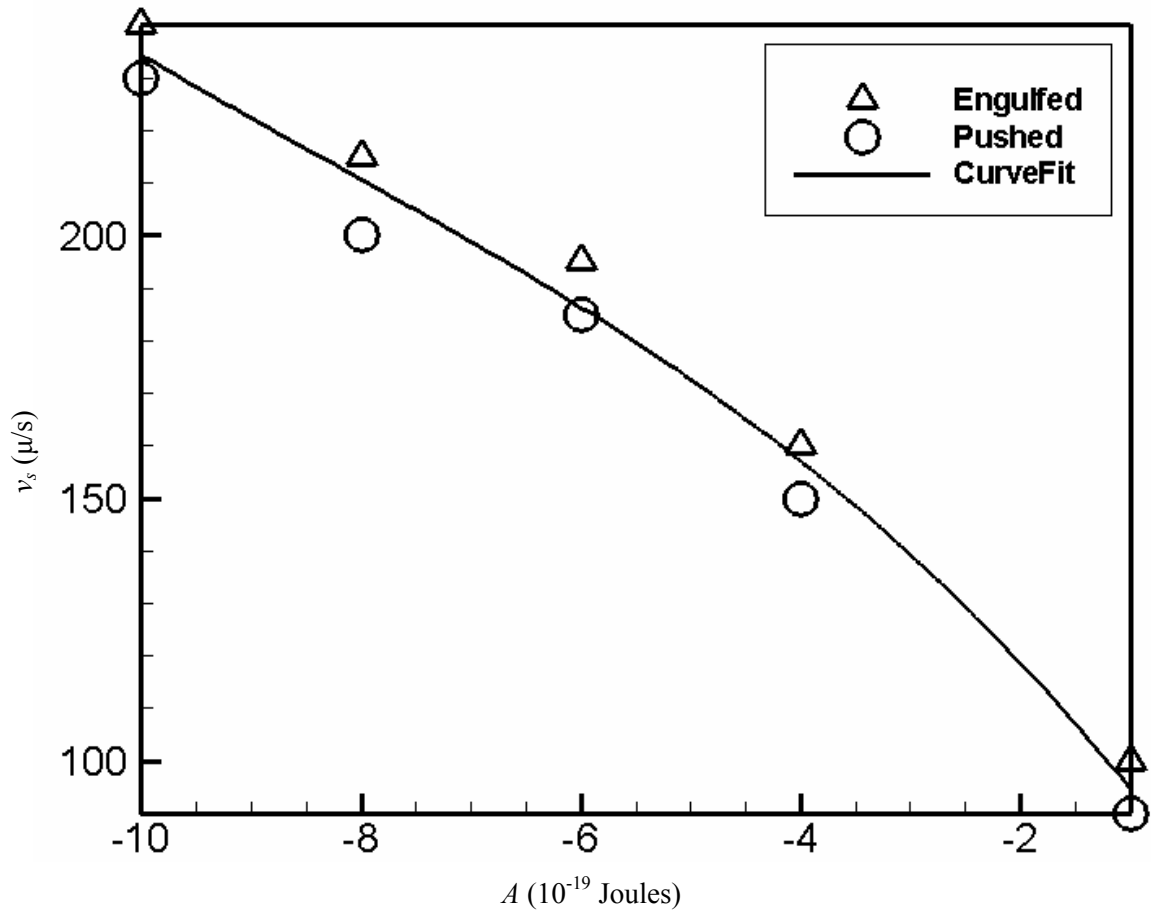


Figure 9: Dependence of the critical velocity on the Hamaker constant, v_s vs. A . The other parameters are held fixed at $k_p/k_l = 0.01$, $R_p = 1.0 \times 10^{-6} \text{ m}$, and $\gamma_{sl} = 0.0$.

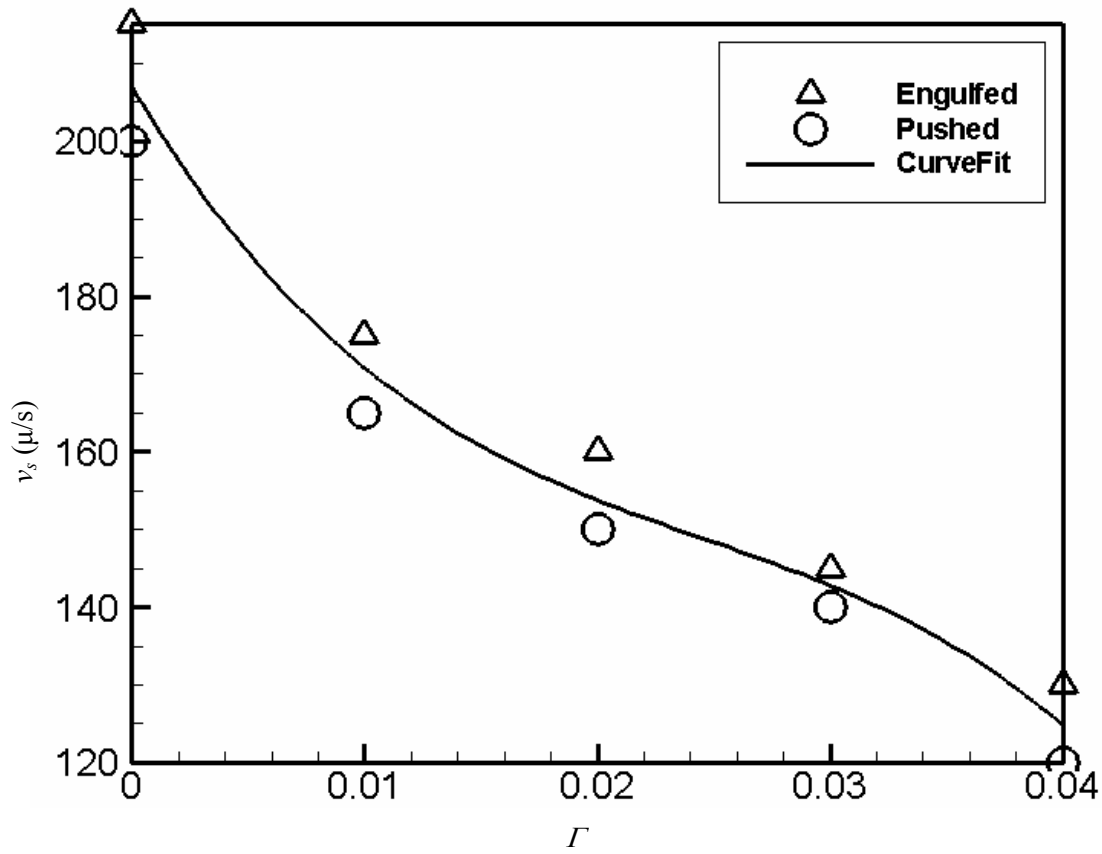


Figure 10: Dependence of the critical velocity on the solid-liquid interface tension, v_s vs. Γ . The values of the other parameters are held fixed at $k_p/k_l = 0.01$, $R_p = 1.0 \times 10^{-6}$ m, $A = -8 \times 10^{-19}$ Joules, $\lambda = 3.5 \times 10^{-10}$ meters.